Erzincan Üniversitesi
Fen Bilimleri Enstitüsü Dergisi
2023, 16(3), 687-713
ISSN: 1307-9085, e-ISSN: 2149-4584
Araştırma Makalesi

Erzincan University
Journal of Science and Technology
2023, 16(3), 687-713
DOI: 10.18185/erzifbed.1324916
Research Article

The Efficiency of Chamomile in Crystal Violet Dye Removal Processes

Sahra DANDIL[1*]

[1*]Department of Chemical Engineering, Faculty of Engineering, Bilecik Şeyh Edebali University, Bilecik, Türkiye

Received: 09/07/2023, **Revised**: 29/09/2023, **Accepted**: 10/10/2023**, Published**: 31/12/2023

Abstract

In this study, the adsorbing properties of chamomile were investigated. Untreated chamomile (Ch) and its activated carbon form (Ch-H_3PO_4) prepared using phosphoric acid (H_3PO_4) were used in Crystal Violet (CV) dye adsorption processes. Scanning Electron Microscopy (SEM) analysis was done to observe the surface structures of the materials. Chemical characterization of Ch and Ch-H_3PO_4 was carried out using Fourier Transform Infrared Spectroscopy (FTIR). Adsorption efficiencies were studied for each material depending on pH (1-7), time (0-300 min), initial concentration of dye (10-50 ppm), amount of adsorbent (0.5-2 g/L) and temperature (25-45 °C) and compared with each other. The time for adsorption processes to reach equilibrium was determined as 300 minutes. The highest removals were obtained at pH 7 in both processes. At all varying concentrations, both materials reached high removal yields. In addition, it was observed that the changing adsorbent dosage greatly affected the capacity values of both materials. The kinetic studies found that the processes were explained by the pseudo-second-order kinetic model and the isotherm studies were compatible with the Freundlich isotherm. In thermodynamic studies, enthalpy (ΔH^0) values were determined as 20.69 and -34.87 kJ mol^{-1} for Ch and Ch-H_3PO_4, respectively. Negative and positive ΔH^0 values indicate exothermic and endothermic nature, respectively. The entropy (ΔS^0) values for Ch and Ch-H_3PO_4 were found to be 76.52 and -95.55 J $mol^{-1}K^{-1}$, respectively. Negative Gibb's free energy (ΔG^0) values explained the spontaneity of the processes. As a result, it was identified that untreated chamomile was effective in CV dye removal, and its effectiveness increased with the preparation of activated carbon using H_3PO_4.

Keywords: Chamomile, Dye, Efficiency, Phosphoric Acid, Untreated

Crystal Violet Boya Giderim Proseslerinde Papatyanın Etkinliği

Öz

Bu çalışmada papatyanın adsorplama özellikleri incelenmiştir. Crystal Violet (CV) boya adsorpsiyon proseslerinde, işlenmemiş papatya (Ch) ve fosforik asit (H_3PO_4) kullanılarak hazırlanan aktif karbon formu (Ch-H_3PO_4) kullanılmıştır. Malzemelerin yüzey yapılarını gözlemlemek için Taramalı Elektron Mikroskobu (SEM) analizi yapılmıştır. Ch ve Ch-H_3PO_4'ün kimyasal karakterizasyonu Fourier Transform Infrared Spektroskopisi (FTIR) ile gerçekleştirilmiştir. Adsorpsiyon etkinlikleri pH (1-7), zaman (0-300 dk), başlangıç boya konsantrasyonu (10-50 ppm), adsorban miktarı (0,5-2 g/L) ve sıcaklığa (25-45 °C) bağlı olarak her bir malzeme için incelenmiş ve birbiriyle karşılaştırılmıştır. Adsorpsiyon proseslerinin dengeye ulaşma süresi 300 dakika olarak belirlenmiştir. Her iki proseste de en yüksek giderimler pH 7' de elde edilmiştir. Tüm değişen konsantrasyonlarda, her iki malzeme de yüksek giderim verimlerine ulaşmıştır. Ayrıca değişen adsorban dozajının, her iki malzemenin kapasite değerlerini büyük ölçüde etkilediği gözlenmiştir. Kinetik çalışmalarda proseslerin yalancı ikinci dereceden kinetik model ile açıklandığı ve izoterm çalışmalarının Freundlich izotermi ile uyumlu olduğu görülmüştür. Termodinamik çalışmalarda entalpi (ΔH^0) değerleri Ch ve Ch-H_3PO_4 için sırasıyla 20,69 ve -34,87 kJ mol^{-1} olarak hesaplanmıştır. Negatif ve pozitif ΔH^0 değerleri sırasıyla ekzotermik ve endotermik doğayı göstermiştir. Ch ve Ch-H_3PO_4 için entropi (ΔS^0) değerleri sırasıyla 76,52 ve -95,55 J $mol^{-1}K^{-1}$ olarak bulunmuştur. Negatif Gibb's serbest enerji (ΔG^0) değerleri proseslerin kendiliğindenliğini açıklamıştır. Sonuç olarak, işlenmemiş papatyanın CV boya gideriminde etkili olduğu, H_3PO_4 kullanılarak aktif karbon hazırlanması ile etkinliğinin arttığı belirlenmiştir.

Anahtar Kelimeler: Boya, Etkinlik, Fosforik Asit, İşlenmemiş, Papatya

*Corresponding Author: sahra.ugur@bilecik.edu.tr
Sahra Uğur, https://orcid.org/0000-0001-9724-5597

1.Introduction

Wastewater is poor-quality water due to dissolved or undissolved contaminants such as industrial (dyes, drugs, heavy metals) or household waste. Due to the decrease in water resources and the increasing need for water, the issue of wastewater treatment has gained importance worldwide. In this context, countries are working on issues such as controlling industrial activities with legal regulations, raising awareness of the public about the correct use of water, preventing excessive water use, and making wastewater reusable. In addition, scientists have focused on water treatment to provide quality water in the most effective and environmentally friendly way. In recent years, many different methods such as electrodeposition [1], ion-exchange [2], adsorption [3], chemical precipitation [4], and membrane [5] have been used for wastewater treatment. In the adsorption method, which is the most preferred technique, the solid surface (adsorbent) retains the pollutant in the aqueous environment. The method has superior features such as ease of operation and control, cost-effectiveness, and reusability of adsorbents with high efficiency [6,7]. The properties of the adsorbent greatly affect the performance of adsorption processes [8]. Among the most used adsorbents such as activated carbons, zeolites, and clays, activated carbon provides high efficiency in adsorption processes [9,10].

Chamomile is a member of the Asteraceae family and is a plant that grows spontaneously or is cultivated in most climates [11]. The most common species known are German chamomile and Roman chamomile [12]. German chamomile (*Matricaria recutita/chamomilla*) is an annual herb with finely divided leaves, while Roman chamomile (*Chamaemelum nobile*) is perennial with threadlike segmented leaves [12,13]. It is known that its use in history dates back to very old civilizations [14]. It is widely used in medicine, to obtain oil, fragrance, and color, and for decorative purposes [15,16].

In this study, the usability of chamomile plants in adsorption processes was investigated. Untreated chamomile and its activated carbon form using phosphoric acid (H_3PO_4) were prepared for use in adsorption. The characteristic surface morphology of untreated chamomile and the appearance of surface structure of the its activated carbon form was demonstrated by Scanning Electron Microscopy (SEM) images. Definition of functional groups of the materials was carried out using Fourier Transform Infrared Spectroscopy (FTIR) analysis. The prepared materials were used in Crystal Violet (CV) dye removal processes and their effectiveness was presented in comparison with each other. CV is a cationic, triaryl methane dye that has many uses in many fields and is known to be quite harmful [17]. The initial pH and concentration, contact time, amount of adsorbent and temperature parameters affecting the adsorption processes were investigated for the processes using each material. The processes were explained by adsorption kinetic and isotherm models. Additionally, thermodynamic analyses were performed based on temperature studies. Since chamomile grow spontaneously, it is easy and cheap to obtain. Thus, it was thought that it could be a cheap and natural adsorbent

alternative. Additionally, according to my best research, the use of the untreated and activated carbon form of chamomile in CV dye adsorption processes has not been found in previous studies.

2. Materials and Methods

2.1. Materials

The chamomile plant (*Matricaria chamomilla*) was supplied by a market in Bilecik. The chemical activation agent, orthophosphoric acid (H_3PO_4, 85%), was provided from Carlo Erba (Cornaredo, Milano, Italy). Sodium hydroxide (NaOH) pellets were also supplied by Carlo Erba (Cornaredo, Milano, Italy). CV dye was purchased from Fluka (Charlotte, North Carolina, United States).

2.2. Preparation and characterization of untreated chamomile and its activated carbon form

Untreated natural chamomile (Ch) and activated carbon obtained by treating chamomile with H_3PO_4 (Ch-H_3PO_4) were prepared to use in dye adsorption processes. The reason why H_3PO_4 is preferred in the preparation of activated carbon is its features such as being non-polluting, cheap and effective [18,19]. Ch was prepared by grinding and sieving natural chamomile. No heat or chemical treatment was applied. To prepare the Ch-H_3PO_4, the widely known activated carbon preparation method, which includes chemical and thermal activation, was used. For this method, a procedure was planned that could use the least amount of energy (chemical activation at room temperature) and chemical (H_3PO_4:chamomile = 2:1 ratio by mass) under known average activation conditions (600 °C, 1h, 10 °C/min, 100 mL/min) similar to previous studies [20-27]. In the preparation of Ch-H_3PO_4, the chamomile was impregnated with H_3PO_4 at a ratio of 2:1 by mass and left at room temperature for 1 day. Then, the mixture was dried. The dried mixture was put into a tubular oven and treated at 600 °C for 1 h at a heating rate of 10 °C/min and a flow rate of 100 mL/min of nitrogen gas. The sample was washed several times with 0.1 M NaOH solution. Then, washing was done with distilled water. The sample was dried at 105 °C overnight.

The surface morphologies of Ch and Ch-H_3PO_4 were studied by SEM (Zeiss Supra 40VP, Oberkochen, Germany) analysis to observe the surface morphology of the untreated chamomile and the changing surface structures in its activated carbon form. Characteristic functional groups of Ch and the status of these groups in Ch-H_3PO_4 were determined by FTIR (Perkin Elmer LR64912C, Waltham, Massachusetts, United States) technique, together with newly formed and disappeared groups.

2.3. Batch adsorption experiments using Ch and Ch-H_3PO_4

Ch and Ch-H_3PO_4 were used in CV dye removal from aqueous medium. The parameters affecting the adsorption processes were determined as pH (1-7), time (0-300 min), initial dye concentration (10-50 ppm), adsorbent dosage (0.5-2 g/L), and temperature (25-45 °C). For the experiments, 50 mL dye solutions were prepared using distilled water. Dye removal experiments were carried out in a Termal H11960 (Başakşehir, İstanbul, Türkiye) shaker at 200 rpm.

The progress of the dye removal processes was followed over time. For this, the concentrations of the samples collected at the specified times were determined. Perkin Elmer, Elmer Analyst 800 (Waltham, Massachusetts, United States) Ultraviolet/Visible region (UV-Vis) spectrophotometer was used to define absorbance of the samples at 590 nm.

It has been observed that Ch gives a yellow color in aqueous environment. For this reason, Ch experiments were carried out with blind samples. For each time and experimental parameter, both blind and standard adsorption processes were performed, absorbance values were determined for both, and the difference between them was taken and recorded as the experimental result.

2.4.Theory

To determine the removal yields of the adsorption processes Equation (1) was used and given below [28]:

$$\text{Removal (\%)} = \frac{(C_0 - C_e)x100}{C_0} \quad (1)$$

C_o and C_e symbolize the concentration values at initial and equilibrium (mg L^{-1}), respectively [28].

Equations (2) and (3) were used to calculate adsorption capacities [29]:

$$q_t = \frac{(C_0 - C_t)xV}{m} \quad (2)$$

$$q_e = \frac{(C_0 - C_e)xV}{m} \quad (3)$$

q_t and q_e symbolize the adsorption capacity at time t and equilibrium (mg g^{-1}), C_t symbolizes the concentration at time t (mg L^{-1}), V symbolizes the solution volume (L), m symbolizes the adsorbent weight (g) [29].

The most commonly known models, pseudo-first-order and pseudo-second-order kinetic models were performed for kinetic studies. The equations of the pseudo-first-order and pseudo-second-order kinetic models are given as Equations (4) and (5), respectively [30]:

$$\log (q_{e-} q_{t}) = \log q_e - (\frac{k_1}{2.303})t \quad (4)$$

$$\frac{t}{q_t} = \frac{1}{k_2 q_e^2} + \frac{t}{q_e} \quad (5)$$

t symbolizes time (min), and k_1 and k_2 symbolize the rate constants of the pseudo-first-order kinetic model (min^{-1}) and pseudo-second-order kinetic model (g mg^{-1} min^{-1}), respectively [30].

Langmuir and Freundlich isotherm models were used to clarify the mechanisms of the processes. Langmuir and Freundlich isotherm model equations are given in Equations (6) and (7), respectively [31]:

$$\frac{C_e}{q_e} = \frac{C_e}{q_m} + \frac{1}{(q_m K_L)} \quad (6)$$

$$\log q_e = \log K_F + \frac{1}{n} \log C_e \quad (7)$$

q_m symbolizes the maximum adsorption capacity (mg g^{-1}), K_L symbolizes the Langmuir isotherm constant (L mg^{-1}), K_F symbolizes the Freundlich isotherm constant (mg g^{-1}) (L $mg^{-1})^{1/n}$), and n symbolizes the parameter for Freundlich isotherm [31].

Thermodynamic studies were also performed for the adsorption processes. Equations (8), (9), (10) and (11) were used to calculate the thermodynamic parameters of the processes [32]:

$$\ln \frac{q_e}{C_e} = \frac{\Delta S^0}{R} - \frac{\Delta H^0}{RT} \quad (8)$$

$$K_e = \frac{q_e}{C_e} \quad (9)$$

$$\Delta G^0 = -RTlnK_e \quad (10)$$

$$\Delta G^0 = \Delta H^0 - T\Delta S^0 \quad (11)$$

ΔS^0 symbolizes the entropy (J $mol^{-1}K^{-1}$), ΔH^0 symbolizes the enthalpy (kJ mol^{-1}), R symbolizes the gas constant (8.314 J mol^{-1} K^{-1}), T symbolizes the temperature (K), K_e symbolizes the adsorption equilibrium constant, ΔG^0 symbolizes Gibb's free energy (kJ mol^{-1}) [32].

3. Results and Discussion

3.1. Surface morphology of Ch and Ch-H_3PO_4

The surface structures of Ch and Ch-H_3PO_4 were examined by SEM analysis. Figure 1 (a) and (b) belong to images of SEM analysis of Ch and Ch-H_3PO_4, respectively. As seen in Figure 1 (a), Ch has a characteristic surface morphology consisting of different structures. SEM image of the activated carbon form of Ch (Figure 1 (b)) exhibited a different surface morphology than that of Ch (Figure 1 (a)). The surface of untreated Ch with a rough structure (Figure 1(a)) became porous after activation (Figure 1(b)). As shown in Figure 1 (b), a large porous and

homogeneous surface structure was obtained in activated carbon prepared using H_3PO_4. It has been emphasized in previous studies that H_3PO_4 treatment in activated carbon synthesis causes large pores on the surface [33]. In addition, it is also mentioned in the literature that with the preparation of activated carbon from the raw material, its morphology changes and pores and holes are formed on the surface [34-36].

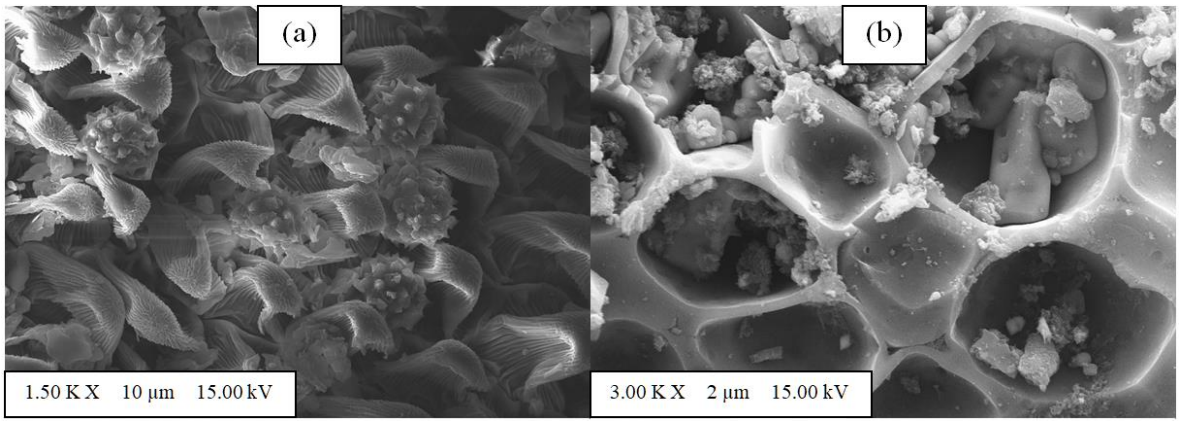

Fig 1. Images of SEM analysis of (a) Ch and (b) Ch-H_3PO_4

3.2.Chemical characterization of Ch and Ch-H_3PO_4

Chemical characterization was studied using FTIR analysis to detect the functional groups of Ch and Ch-H_3PO_4. Figures 2 (a) and (b) show the FTIR spectra of Ch and Ch-H_3PO_4, respectively.

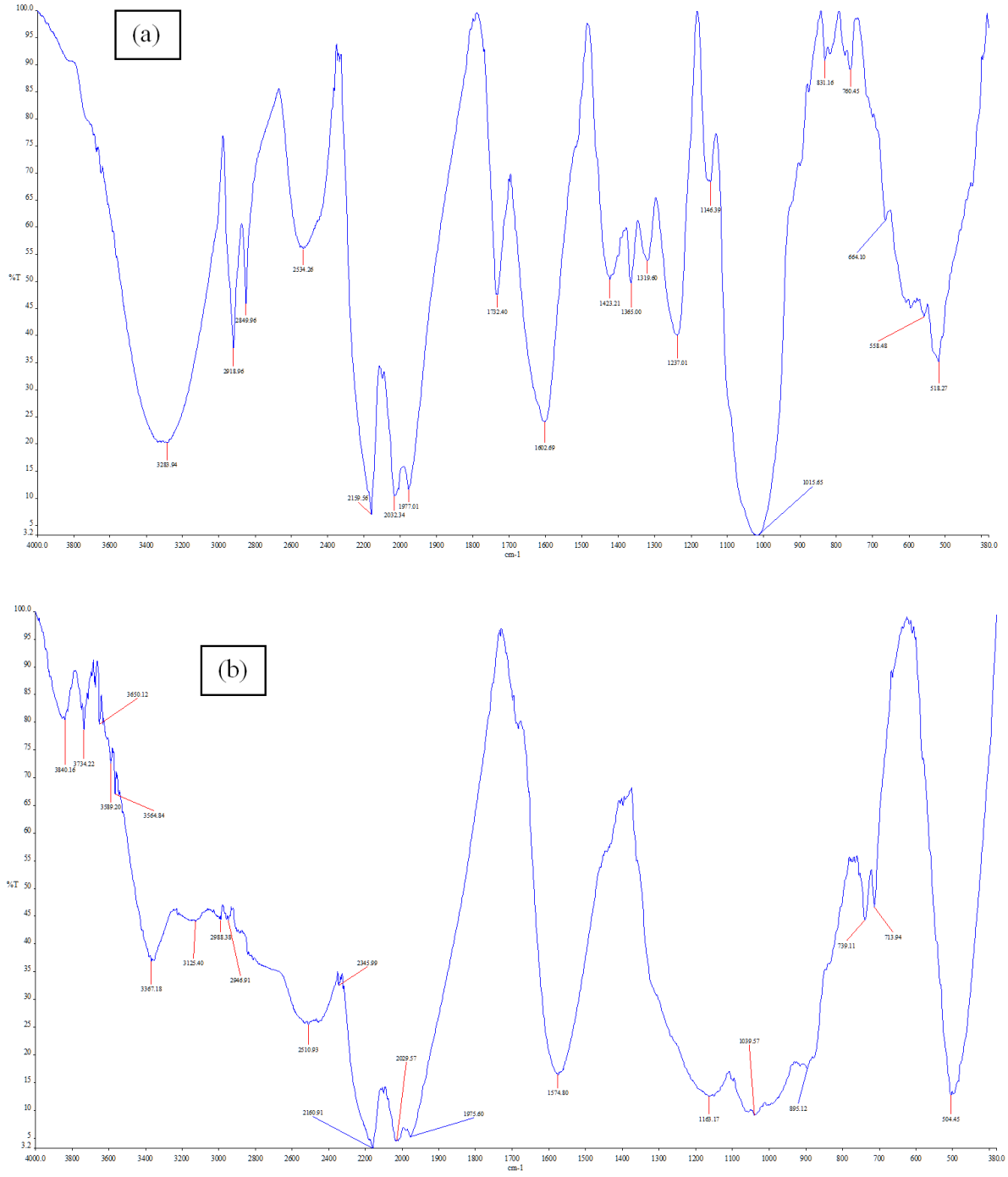

Fig 2. FTIR spectra of (a) Ch and (b) Ch-H_3PO_4

The 3283 cm^{-1} peak seen in the spectra of untreated Ch in Figure 2 (a) indicates the presence of O-H groups [37,38]. The peaks at 2918 and 2849 cm^{-1} show to C-H groups [39]. It was reported by Fernandes et al. that plants belonging to the Asteraceae family, including chamomile, contain S [40], and therefore the 2534 cm^{-1} peak may belong to the thiol group [41,42]. Peaks caused by –CO groups are seen at 2159 and 2032 cm^{-1} [43-45]. The 1977 cm^{-1} peak may belong to the vibrations of C-H groups [46]. The 1732 cm^{-1} peak indicates C=O groups [47]. COO^- groups have a peak at 1602 cm^{-1} [48]. The peaks at 1423 and 1365 cm^{-1} belong to C-H groups [49,50]. The 1319 cm^{-1} peak may indicate the =C-H group [51]. The peaks in the range of 1237-1015 cm^{-1} belong to C-O vibrations [52-54]. The 831 cm^{-1} peak indicates the =C-H group [55]. For the chamomile plant, which contains aromatic compounds [56], the 760 cm^{-1} peak may belong to the benzene ring [57].

In the FTIR spectra of Ch-H_3PO_4 (Figure 2 (b)), which was obtained by chemically activating untreated Ch with H_3PO_4 and turning it into activated carbon, some peaks belonging to Ch shifted due to activation, while new peaks were formed or existing peaks disappeared. In the study conducted by Mohtashami et al. [58], activated carbon obtained using H_3PO_4 showed the formation of many peaks in the region above 3300 cm^{-1} compared to its untreated form. Similar to Mohtashami et al., the 3840-3564 cm^{-1} peaks seen in Figure 2 (b) may belong to the O-H groups of phenolic and carboxylics and adsorbed water with H_3PO_4 treatment [58]. While the peaks at 1732 and 1602 cm^{-1} seen in Figure 2 (a) were not observed for Ch-H_3PO_4, a peak was observed at 1574 cm^{-1}, which may belong to C=C [59]. It is also seen that the strong peaks seen for Ch in the range of approximately 1500-1200 cm^{-1} have lost their effect. The peaks at 1163 and 1039 cm^{-1} may indicate P=O and P-O-C groups caused by H_3PO_4 treatment [60-62].

3.3. Effect of the contact time and pH of CV dye solution

The contact time study of CV dye adsorption processes using Ch and Ch-H_3PO_4 was carried out depending on each pH value. The CV dye solutions pH was adjusted to 1, 3, 5, and 7, and the percentages of removal over time were followed in the process performed with each material. Experimental parameters were determined as 20 ppm initial CV dye concentration, 1 g/L adsorbent dosage, and room temperature. Figures 3 (a) and (b) show the change in removal yields of CV dye over time for Ch and Ch-H_3PO_4, respectively.

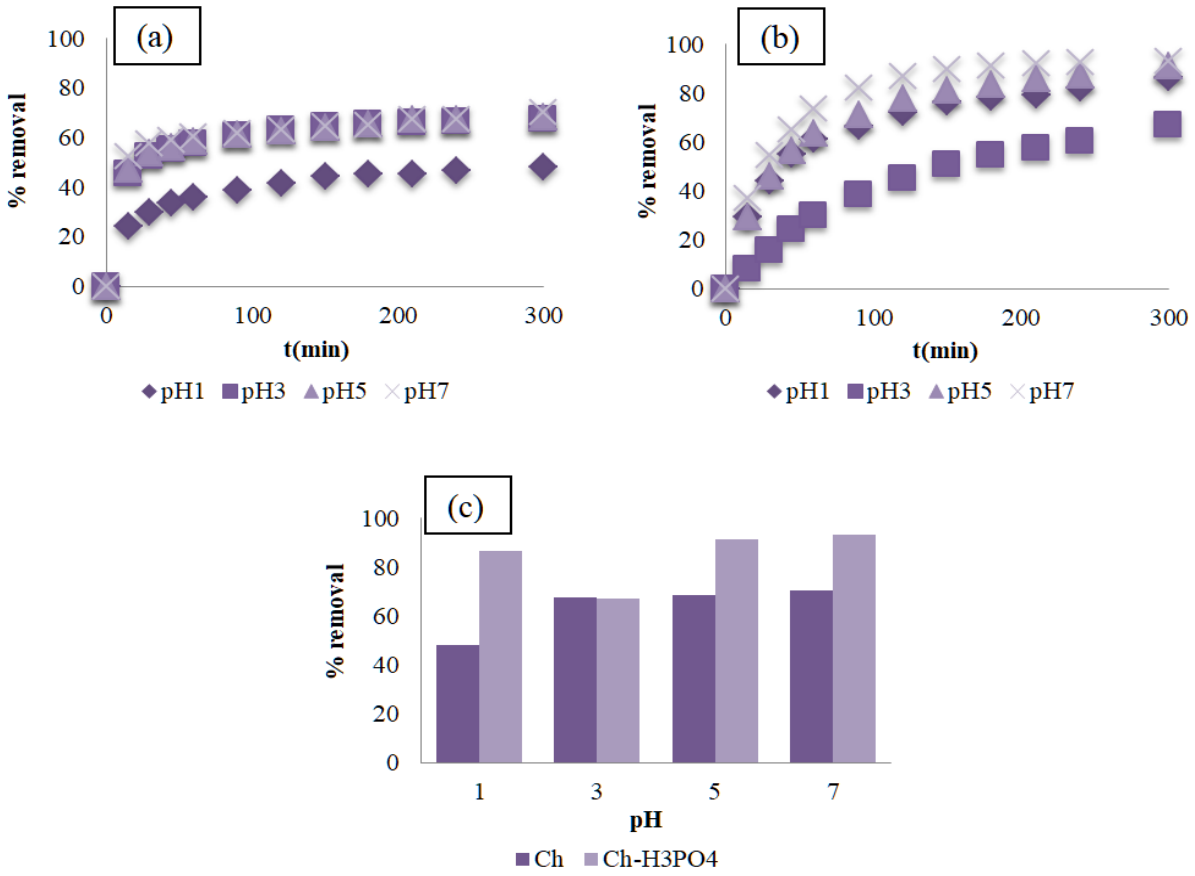

Fig 3. Percentages of removal over time for (a) Ch and (b) Ch-H_3PO_4, and (c) pH-% removal graph for Ch and Ch-H_3PO_4

According to Figures 3 (a) and (b), all processes exhibited regular removal behavior at each pH value. In addition, adsorption was rapid in the early times of each process. Again, as seen in Figures 3 (a) and (b), for the adsorption behavior of the processes over time, there started to be slight changes in the removal yields of CV dye adsorption processes using Ch and Ch-H_3PO_4 towards the end of the monitored time. The flattening of the last parts of the curves in Figures 3 (a) and (b) shows this situation. When the removal yields in both processes were followed up to 300 minutes, no significant change was observed in the results for the last time. Thus, the equilibrium times of the processes were determined as 300 minutes.

Figure 3 (c) shows the CV dye removal yields using Ch and Ch-H_3PO_4 at different pH values at the end of 300 minutes and compares them with each other. Removal yields of 48.35, 67.35, 68.34, and 70.38% were obtained for Ch at pH 1, 3, 5, and 7, respectively. Ch-H_3PO_4 provided 86.49, 66.95, 91.08, and 93.11% removal yields at pH 1, 3, 5, and 7, respectively. The highest adsorption yields were determined at pH 7 for adsorption processes using Ch and Ch-H_3PO_4. Providing high efficiency without harsh pH conditions was seen as the advantage of the process. As shown in Figure 3 (c), the highest percentage values were obtained for Ch-H_3PO_4 at all pH values studied. According to this; it was determined that H_3PO_4 treatment of natural chamomile improved the adsorption properties of the material. It is also worth noting the effective adsorption behavior of untreated natural chamomile (Ch).

3.4. Effect of the initial CV dye concentration

For the CV dye removal processes using Ch and Ch-H_3PO_4, experiments were carried out for 10, 20, 30, 40, and 50 ppm CV dye concentrations to exhibit the effect of varying CV concentration in aqueous solution on removal yields. Experiments were performed at pH 7 where the highest removal yields were determined for the materials. Studies were followed for 300 minutes, which was determined as the equilibrium time for the processes, at 1 g/L adsorbent dosage and room temperature. The results are presented in Figure 4.

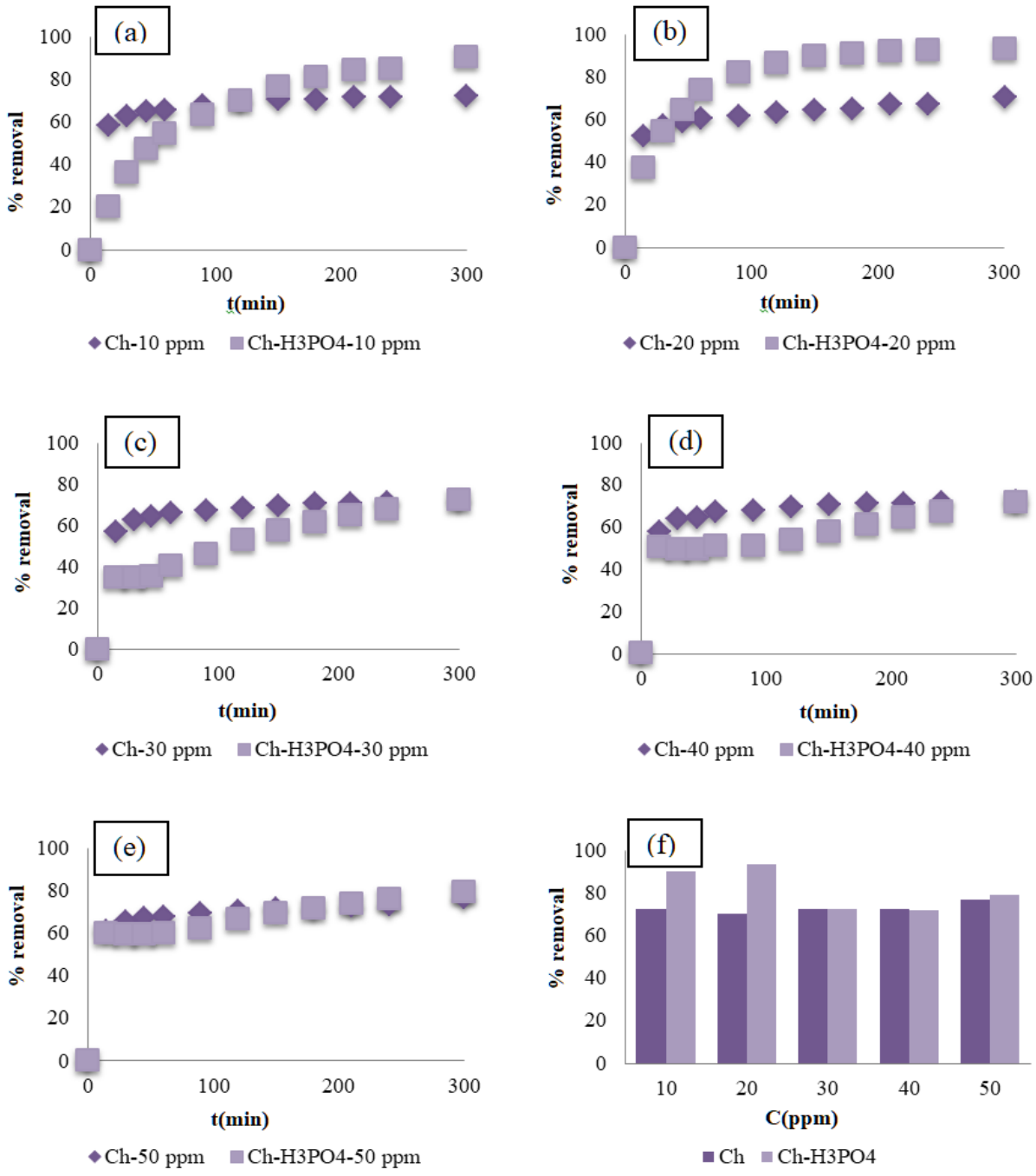

Fig 4. Removal yields of Ch and Ch-H_3PO_4 at (a) 10, (b) 20, (c) 30, (d) 40, and (e) 50 ppm, and (f) concentration (C)-% removal graph for Ch and Ch-H_3PO_4

Figure 4 (a), (b), (c), (d), and (e) show the removal efficiencies of adsorption processes using Ch and Ch-H_3PO_4 overtime at 10, 20, 30, 40 and 50 ppm CV dye concentrations, respectively. According to Figure 4 (a-e), Ch showed similar removal yields at all concentrations. It provided high removal yields of 72.53, 70.38, 72.17, 72.52, and 76.61% at 10, 20, 30, 40, and 50 ppm, respectively. Accordingly, it can be said that Ch can offer sufficient capacity for all concentration values. On the other hand, Ch-H_3PO_4 reached high removal values. Ch-H_3PO_4 provided 90.27, 93.11, 72.39, 72.01, and 79.25% CV removal yields at 10, 20, 30, 40, and 50 ppm, respectively. For Ch-H_3PO_4, this is because active sites that are sufficient for low concentrations become saturated at high concentrations [63,64]. These results indicate that the highest efficiency was obtained with Ch-H_3PO_4, similar to the results of the pH-time study. In addition, Figure 4 (f) refers to the percentage of removal of Ch and Ch-H_3PO_4 at varying CV dye concentrations. Figure 4 (f) indicates that Ch-H_3PO_4 provides the highest removals at 10 and 20 ppm, while Ch and Ch-H_3PO_4 achieve similar removal efficiency at 30, 40, and 50 ppm.

3.5. Effect of the Ch and Ch-H_3PO_4 dosage

The changes in removal yield values and adsorption capacities for CV dye removal processes using Ch and Ch-H_3PO_4 at varying adsorbent dosages were investigated. The experiments were performed at 0.5, 1, and 2 g/L adsorbent dosages for 20 ppm dye concentration, 300 minutes, room temperature, and pH 7. Figure 5 shows the removal yields and adsorption capacities together at varying adsorbent dosages for dye adsorption processes using Ch and Ch-H_3PO_4.

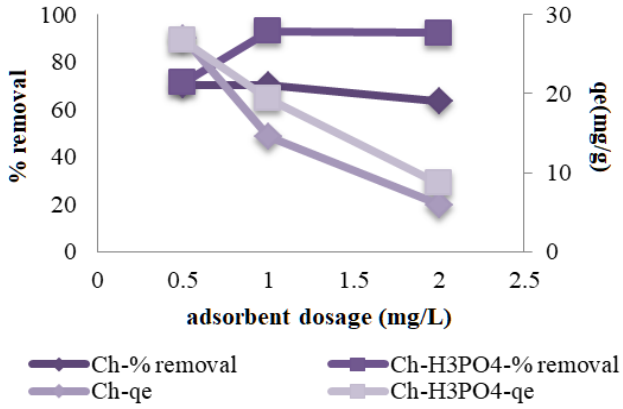

Fig 5. Removal yields and adsorption capacities for adsorption processes using Ch and Ch-H_3PO_4 depending on the adsorbent dosage

For Ch, at 0.5, 1, and 2 g/L adsorbent dosage, the removal rates were 70.15, 70.38, and 63.56% while the adsorption capacities were 27.08, 14.61, and 5.97 mg/g, respectively. While the dosage of Ch-H_3PO_4 was 0.5, 1, and 2 g/L, the removal yields were 71.43, 93.11, and 92.23 and the adsorption capacities were determined as 26.73, 19.3, and 8.61 mg/g, respectively. Accordingly, Ch-H_3PO_4 exhibited higher removal and adsorption capacity than Ch at each adsorbent dosage. In addition, it was determined that the capacities decreased as the adsorbent dosage increased for both Ch and Ch-H_3PO_4.

Although the capacity decreases when the adsorbent dosage is varied from 0.5 g/L to 1 g/L for both adsorbents, it has been interpreted that the increased amount of adsorbent per L solution volume encourages the removal yields. When the adsorbent dosage for Ch and Ch-H_3PO_4 varied from 1 g/L to 2 g/L, the capacities again decreased, but the removal yield for Ch was noticeably lowered, while a slight decrease was observed for Ch-H_3PO_4. In this case, it can be said that the significant decrease in the capacity of the Ch and Ch-H_3PO_4 is slightly effective on the removal yields.

3.6. Adsorption kinetics

Kinetic studies for the CV dye removal processes using Ch and Ch-H_3PO_4 were carried out by pseudo-first-order kinetic model and pseudo-second-order kinetic model. Figure 6 presents the graphs of the kinetic models.

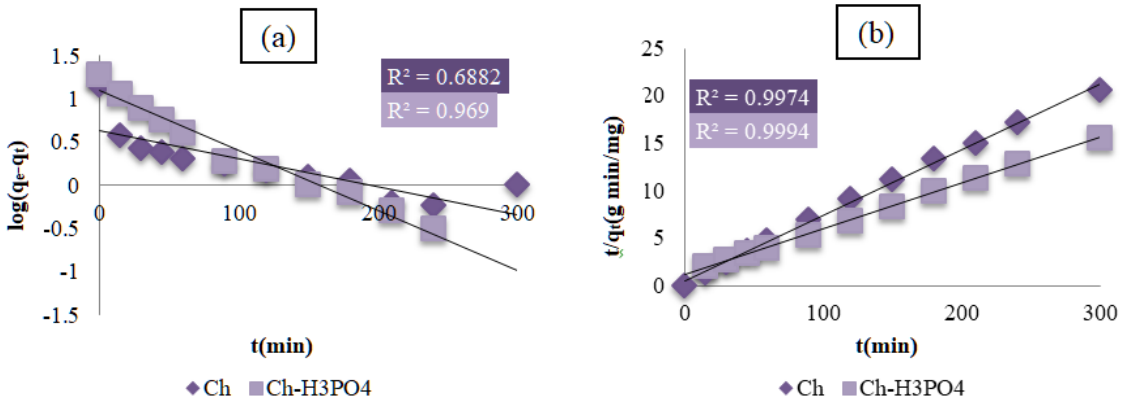

Fig 6. Graphs of (a) pseudo-first-order and (b) pseudo-second-order kinetic models

The compatibility of the adsorption processes with the kinetic models was evaluated by the regression coefficient (R^2). Since the highest R^2 values belonged to the most compatible model, it was determined that the pseudo-second-order kinetic model best explained the CV dye adsorption processes using Ch and Ch-H_3PO_4. Chemical adsorption occurs in processes that fit the pseudo-second-order kinetic model [65]. In chemical adsorption processes, chemical bond formation occurs between the adsorbent surface and the component in the aqueous medium [66]. Table 1 represents the kinetic parameters of the pseudo-first-order and pseudo-second-order models. According to Table 1, the experimental qe values of both processes were found to be close to the qe values calculated for the pseudo-second order model. The closest values support the fit of the processes to the model. The values of q_e for the pseudo-second-order kinetic model appear to be greater for Ch-H_3PO_4 than for Ch for the adsorption processes.

Table 1. Parameters of the kinetic models

		Pseudo-First Order Kinetic Model			Pseudo-Second Order Kinetic Model		
	$q_{e,\ exp}$ (mg g^{-1})	k_1 ($x10^3$) (min^{-1})	$q_{e,\ cal}$ (mg g^{-1})	R^2	k_2 ($x10^3$) (g mg^{-1} min^{-1})	$q_{e\ ,cal}$ (mg g^{-1})	R^2
Ch	14.61	7.37	4.33	**0.6882**	8.63	14.53	**0.9974**
Ch-H_3PO_4	19.3	15.89	12.56	**0.969**	1.99	20.79	**0.9994**

3.7. Adsorption isotherms

Adsorption equilibrium studies were evaluated using Langmuir and Freundlich isotherm models. The models were applied to explain the mechanisms of CV dye removal processes using Ch and Ch-H_3PO_4. Figure 7 (a) and (b) are graphs of Langmuir and Freundlich isotherm models, respectively.

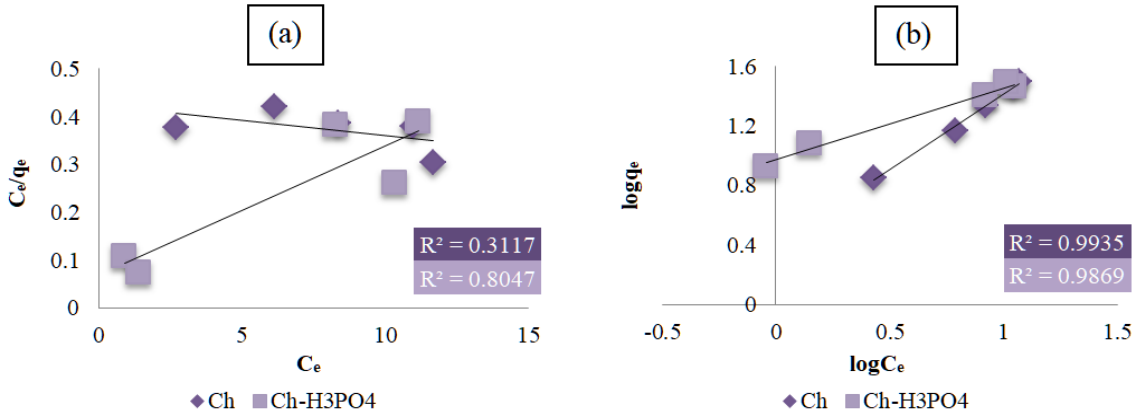

Fig 7. Graphs of (a) Langmuir and (b) Freundlich isotherm models

According to the highest R^2 values given in Figure 7, the processes were found to be compatible with the Freundlich isotherm model. Freundlich isotherm model explains that because of the active sites with different energies, uniform adsorption cannot occur, so multilayer adsorption occurs [67]. In addition, the parameters of the isotherm models are presented in Table 2. Isotherm parameters were obtained using the slope and intercept of the lines in the graphs given in Figure 7. In Figure 7 (a), where the Langmuir isotherm of the process using Ch is shown, it can be seen that the line is downwards. This means that the slope of the line is negative and therefore explains that the values of K_L and q_m are found to be negative. Since Ce/qe values that are not proportional to Ce values were obtained based on experimental studies, the Ce/qe - Ce line for the process using Ch in Figure 7 (a) is downwards. Table 2 shows that the K_F values

for Ch and Ch-H_3PO_4 are 2.51 and 9.41, respectively. The K_F value is a parameter in a relation with the capacity, and accordingly, the adsorption capacity for the Ch-H_3PO_4 process is greater than that of the Ch process [68]. For another parameter, n; if 1/n is less than 1, favorable adsorption occurs [69].

Table 2. Parameters of the isotherm models

	Langmuir Isotherm			**Freundlich Isotherm**		
	K_L(x10^2) (L mg^{-1})	**q_m (mg g^{-1})**	**R^2**	**K_F (mg g^{-1}) (L mg^{-1})$^{1/n}$)**	**n**	**R^2**
Ch	-1.51	-156.25	**0.3117**	2.51	0.98	**0.9935**
Ch-H_3PO_4	39.07	37.037	**0.8047**	9.41	2.08	**0.9869**

3.8. Effect of the temperature and adsorption thermodynamics

The temperature effect on CV dye adsorption processes from aqueous solutions using Ch and Ch-H_3PO_4 were investigated and thermodynamic analyses were carried out accordingly. Experiments were carried out at pH 7, at 1 g/L adsorbent dosage, at 20 ppm CV dye concentration, at 25, 35, and 45 °C for 300 min. The graph of ln(qe/Ce)-1/T for the processes is given in Figure 8.

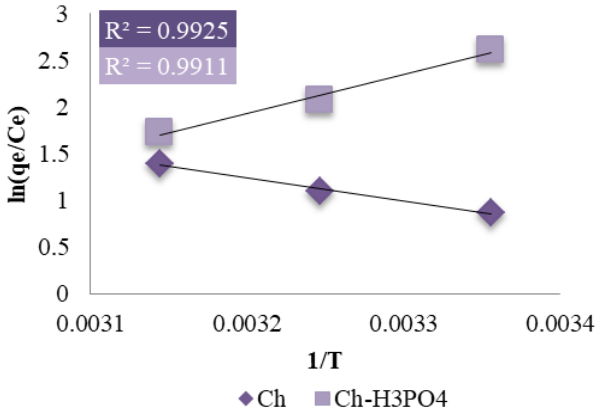

Fig 8. ln(q_e/C_e)-1/T graph

According to Figure 8, high R^2 values were obtained for the processes. Table 3 lists the values of the thermodynamic parameters of each process. As seen in Table 3, the ΔH^0 values are 20.69 and -34.87 kJ mol^{-1} for adsorption processes using Ch and Ch-H_3PO_4, respectively. Negative ΔH^0 values describe the process as exothermic, while positive values indicate the endothermic process [70,71]. The ΔS^0 values for the processes using Ch and Ch-H_3PO_4 were found to be 76.52 and -95.55 J mol^{-1}K^{-1}, respectively. A positive ΔS^0 explains the increasing randomness at the interface [72]. The negative ΔS^0 value explains the increased regularity on the adsorbent

surface [73]. The negative ΔG^0 explains the spontaneity of the processes [74]. The decrease in the absolute ΔG^0 value with increasing temperature indicates that the removal efficiency decreases at higher temperatures for the process [75]. For the adsorption process using Ch, the absolute ΔG^0 increased with temperature, while it decreased for the process using Ch-H_3PO_4. The efficiency of the adsorption process using Ch increases with increasing temperature but decreases for the process using Ch-H_3PO_4.

Table 3. Thermodynamic parameters

	T, K	ΔG^0, kJ mol^{-1}	ΔH^0, kJ mol^{-1}	ΔS^0, J mol^{-1}K^{-1}
Ch	298	-2.11	20.69	76.52
	308	-2.88		
	318	-3.64		
Ch-H_3PO_4	298	-6.39	-34.87	-95.55
	308	-5.44		
	318	-4.48		

3.9. Comparison with similar studies

The experimental q_e, pseudo-second-order kinetic model constant, k_2 and thermodynamic parameters of the processes in which CV dye adsorption studies were previously conducted with natural materials in untreated or activated carbon form, which were compatible with the pseudo-second-order kinetic model, were compared with the parameters of this study. The mentioned parameters in this study and previous studies are given in Table 4.

Table 4. Comparison of $q_{e,exp}$, k_2, ΔG^0, ΔH^0 and ΔS^0 values of this study with previous studies

Activated carbon	$q_{e,exp}$ mg/g	k_2 g mg^{-1} min^{-1}	T K	ΔG^0 kJ mol^{-1}	ΔH^0 kJ mol^{-1}	ΔS^0 J mol^{-1}K^{-1}	Ref.
***Valeriana officinalis* roots**	-	192.3 (25◦C)	298	-31.8	−46.3	−48.6	[69]
		192.3 (35◦C)	308	-31.3			
		192.3 (45◦C)	318	-30.8			
		188.7 (55◦C)	328	-30.4			
Eucalyptus leaves	21.48	0.0046	298 308 318	-4.485 -5.443 -6.128	20.037	82.434	[76]
Date seed powder	-	7.61	298 308 318	−7.678 −8.739 −10.068	5.0249	46.23	[77]
***Rhizophora mucronata* stem-barks**	407.2990	0.0033	-	-	-	-	[78]
***Carpobrotus edulis* plant**	3.562 (20 mg/L) 17.703 (100 mg/L)	0.184 (20 mg/L) 0.045 (100 mg/L)	-	-	-	-	[79]
***Azadirachta indica* (neem) sawdust**	97.58 (1.5 g/L)	0.16	-	-	-	-	[17]
	98.17 (2 g/L)	0.81					
	99.86 (2.5 g/L)	3.42					
	98.82 (100 mg/L)	3.15					
	98.66 (150 mg/L)	1.10					
	96.95 (200 mg/L)	0.14					
	97.49 (25◦C)	0.31					

	97.78 (35◦C)	0.56					
	98.12 (45◦C)	0.78					
Phosphoric and activated male flowers coconut tree	4.900 (10 ppm)	-	301	-77.815	71.490	258.76	[80]
	9.495 (20 ppm)		306	-79.109			
	14.460 (30 ppm)		311	-80.403			
	18.500 (40 ppm)		316	-81.697			
			317	-82.990			
Sulphuric acid activated male flowers coconut tree	11.538 (10 ppm)	-	301	-32.403	73.382	107.896	
	16.134 (20 ppm)		306	-32.942			
	21.456 (30 ppm)		311	-33.482			
	24.450 (40 ppm)		316	-34.022			
			317	-34.561			
Activated carbon prepared from Moroccan *Moringa oleifera* wastes	189.447 (250 mg/L)	$14.714x10^{-4}$ (250 mg/L)	298	−2.044	17.028	0.064	[10]
	345.220 (500 mg/L	$8.3051x10^{-4}$ (500 mg/L)	303	−2.364			
	415.781 (750 mg/L)	$6.1932x10^{-4}$ (750 mg/L)	313	−3.004			
			323	−3.644			
Activated carbon derived from chitin	98.662 (25◦C)	$2.204 x10^{3}$ (25◦C)	298	-1.837	38.949	136.797	[81]
	99.032 (35◦C)	$2.425 x10^{3}$ (35◦C)	308	-3.205			
	99.400 (45◦C)	$1.583 x10^{3}$ (45◦C)	318	-4.573			
Activated *Citrus limetta* peel	-	0.0006	-	-	-	-	[82]
Activated carbon from poultry litter	1.4725	0.1156	-	-	-	-	[83]
Hydrochloric acid-activated coconut flower sheath	4.7521	6.1702	-	-	-	-	[84]

Phosphoric acid activated coconut flower sheath	4.8131	3.6796	-	-	-	-	
			298	-2.11			
Ch	27.08	8.63 x10^{-3}	308	-2.88	20.69	76.52	
			318	-3.64			Present
			298	-6.39			study
Ch-H_3PO_4	26.73	1.99 x10^{-3}	308	-5.44	-34.87	-95.55	
			318	-4.48			

According to the $q_{e,exp}$ values in Table 4, although previous studies included low capacity values [79] for untreated materials, high values [78] were also encountered, and the other relevant studies exhibited capacities in this range. According to these values, it was determined that Ch had an average capacity value. As for the adsorption capacities of activated carbon forms, the capacity values were distributed in a wide range, similar to the untreated materials, and it was observed that Ch-H_3PO_4 again exhibited an average capacity. Additionally, rate constants similar to k_2 values for the processes using Ch and Ch-H_3PO_4 are also included in Table 4. The processes using Ch and Ch-H_3PO_4 exhibited different behaviors in thermodynamic studies. According to the results of thermodynamic studies, the CV dye removal process with Ch is endothermic, its efficiency increases with increasing temperature and disorder at the interface increases, while the process carried out with Ch-H_3PO_4 is exothermic, its efficiency decreases with increasing temperature and it exhibits decreasing disorder at the interface. Adsorptions occurring in accordance with the both processes are seen in Table 4.

4. Conclusion

The study aimed to research the adsorption properties of chamomile. Untreated natural chamomile (Ch) and its activated carbon form (Ch-H_3PO_4) were used in CV dye adsorption. The surface structures of Ch and Ch-H_3PO_4 were investigated by SEM analysis. SEM images showed the characteristic morphology of Ch and the porous structure of Ch-H_3PO_4. The peaks belonging to the functional groups of Ch and the changes in the peaks with activation were revealed by FTIR analysis. The effective parameters (pH of CV dye solution, contact time, initial CV dye concentration, dosage of Ch and Ch-H_3PO_4 and temperature) of the processes were also examined. The processes reached equilibrium in 300 minutes. In both processes, the highest removals were detected at pH 7. The highest adsorption yields in the processes using Ch and Ch-H_3PO_4 were determined as 70.38 and 93.11%, respectively. Ch and Ch-H_3PO_4 achieved high removal yields at all concentrations studied. It was observed that the Ch and Ch-H_3PO_4 dosage was quite effective on the adsorption capacity. Kinetic studies revealed that the processes fit the pseudo-second-order kinetic model. Isotherm studies were examined with Langmuir and Freundlich models. The R^2 value of the Freundlich isotherm model was found to be higher than the Langmuir model for both processes. While the ΔH^0 value of 20.69 kJ mol^{-1} for Ch indicates an endothermic process, the value of -34.87 kJ mol^{-1}, which explains the exothermic nature of Ch-H_3PO_4, was calculated. A positive ΔS^0 value for Ch (76.52 J $mol^{-1}K^{-1}$)

indicated the increasing randomness at the interface. For Ch-H_3PO_4 negative ΔS^0 (-95.55 J $mol^{-1}K^{-1}$) clarified the increased regularity on the adsorbent surface. According to the results, the activated carbon of chamomile using H_3PO_4 provided high removal yields, in addition, a remarkable CV dye adsorption was achieved by untreated natural chamomile.

Ethics in Publishing

There are no ethical issues regarding the publication of this study.

References

[1] Li, S., Dai, M., Ali, I., Bian, H., & Peng, C., (2023) A new idea for efficient copper recovery from wastewater by electrodeposition: Adsorption pretreatment, Desalination, 562, 116683.

[2] Medri, V., Papa, E., Landi, E., Maggetti, C., Pinelli, D., & Frascari, D., (2022) Ammonium removal and recovery from municipal wastewater by ion exchange using a metakaolin K-based geopolymer, Water Research, 225, 119203.

[3] Shourije, S. M. J. S., Dehghan, P., Bahrololoom, M. E., Cobley, A. J., Vitry, V., Azar, G. T. P., ... & Mesbah, M., (2023) Using fish scales as a new biosorbent for adsorption of nickel and copper ions from wastewater and investigating the effects of electric and magnetic fields on the adsorption process, Chemosphere, 137829.

[4] Oh, M., Lee, K., Jeon, M. K., Foster, R. I., & Lee, C. H., (2023) Chemical precipitation–based treatment of acidic wastewater generated by chemical decontamination of radioactive concrete, Journal of Environmental Chemical Engineering, 110306.

[5] da Silva, A. F. V., da Silva, J., Vicente, R., Ambrosi, A., Zin, G., Di Luccio, M., & de Oliveira, J. V., (2023) Recent advances in surface modification using polydopamine for the development of photocatalytic membranes for oily wastewater treatment, Journal of Water Process Engineering, 53, 103743.

[6] de Andrade, J. R., Oliveira, M. F., da Silva, M. G., & Vieira, M. G., (2018) Adsorption of pharmaceuticals from water and wastewater using nonconventional low-cost materials: a review, Industrial & Engineering Chemistry Research, 57(9), 3103-3127.

[7] Wang, B., Lan, J., Bo, C., Gong, B., & Ou, J., (2023) Adsorption of heavy metal onto biomass-derived activated carbon, RSC advances, 13(7), 4275-4302.

[8] Zahid, M., Nadeem, N., Tahir, N., Majeed, M. I., Naqvi, S. A. R., & Hussain, T., (2020) Multifunctional hybrid nanomaterials for sustainable agri-food and ecosystems. Kamel A. Abd-Elsalam (Ed.), Hybrid nanomaterials for water purification (pp. 155-188). Elsevier, Netherlands.

[9] Ho, S., (2022) Low-Cost Adsorbents for the Removal of Phenol/Phenolics, Pesticides, and Dyes from Wastewater Systems: A Review, Water, 14(20), 3203.

[10] Raji, Y., Nadi, A., Mechnou, I., Saadouni, M., Cherkaoui, O., & Zyade, S., (2023) High adsorption capacities of crystal violet dye by low-cost activated carbon prepared from Moroccan Moringa oleifera wastes: Characterization, adsorption and mechanism study, Diamond and Related Materials, 135, 109834.

[11] Sah, A., Naseef, P. P., Kuruniyan, M. S., Jain, G. K., Zakir, F., & Aggarwal, G., (2022) A Comprehensive Study of Therapeutic Applications of Chamomile, Pharmaceuticals, 15(10), 1284.

[12] Bokelmann, J. M., (2022) Medicinal Herbs in Primary Care. Jean M. Bokelmann (Ed.), 35-Chamomile, German (Matricaria recutita/chamomilla) and Chamomile, Roman (Chamaemelum nobile): Flower (pp. 269-277). Elsevier, Netherlands.

[13] Nemecz, G., (1999) Chamomile, Journal of Modern Pharmacy, 6(8), 32.

[14] Ross, S. M., (2008) Chamomile: a spoonful of medicine, Holistic Nursing Practice, 22(1), 56-57.

[15] Kolanos, R., & Stice, S. A., (2021) Nutraceuticals. Ramesh C. Gupta, Rajiv Lall and Ajay Srivastava(Ed.), German chamomile (pp. 757-772). Academic Press, Elsevier, Netherlands.

[16] Chaves, P. F. P., Iacomini, M., & Cordeiro, L. M., (2019) Chemical characterization of fructooligosaccharides, inulin and structurally diverse polysaccharides from chamomile tea, Carbohydrate polymers, 214, 269-275.

[17] Dar, M. A., Anas, M., Kajal, K., Kumar, S., & Kaushik, G. (2023) Adsorptive removal of crystal violet dye by Azadirachta indica (neem) sawdust: A low-cost bio-sorbent, Acta Ecologica Sinica, https://doi.org/10.1016/j.chnaes.2023.02.011.

[18] Reza, M. S., Yun, C. S., Afroze, S., Radenahmad, N., Bakar, M. S. A., Saidur, R., ... & Azad, A. K. (2020) Preparation of activated carbon from biomass and its' applications in water and gas purification, a review, Arab Journal of Basic and Applied Sciences, 27(1), 208-238.

[19] Neme, I., Gonfa, G., & Masi, C. (2022) Activated carbon from biomass precursors using phosphoric acid: A review, Heliyon, 8, e11940.

[20] Gerçel, Ö., & Gerçel, H. F. (2007) Adsorption of lead (II) ions from aqueous solutions by activated carbon prepared from biomass plant material of Euphorbia rigida, Chemical engineering journal, 132(1-3), 289-297.

[21] Xue, H., Wang, X., Xu, Q., Dhaouadi, F., Sellaoui, L., Seliem, M. K., ... & Li, Q. (2022) Adsorption of methylene blue from aqueous solution on activated carbons and composite prepared from an agricultural waste biomass: A comparative study by experimental and advanced modeling analysis, Chemical engineering journal, 430, 132801.

[22] García-Mateos, F. J., Ruiz-Rosas, R., Marqués, M. D., Cotoruelo, L. M., Rodríguez-Mirasol, J., & Cordero, T. (2015) Removal of paracetamol on biomass-derived activated carbon: Modeling the fixed bed breakthrough curves using batch adsorption experiments, Chemical engineering journal, 279, 18-30.

[23] Liou, T. H. (2010) Development of mesoporous structure and high adsorption capacity of biomass-based activated carbon by phosphoric acid and zinc chloride activation, Chemical Engineering Journal, 158(2), 129-142.

[24] Jiang, D., Li, H., Cheng, X., Ling, Q., Chen, H., Barati, B., ... & Wang, S. (2023) A mechanism study of methylene blue adsorption on seaweed biomass derived carbon: From

macroscopic to microscopic scale, Process Safety and Environmental Protection, 172, 1132-1143.

[25] Valdés-Rodríguez, E. M., Mendoza-Castillo, D. I., Reynel-Ávila, H. E., Aguayo-Villarreal, I. A., & Bonilla-Petriciolet, A. (2022) Activated carbon manufacturing via alternative Mexican lignocellulosic biomass and their application in water treatment: Preparation conditions, surface chemistry analysis and heavy metal adsorption properties, Chemical Engineering Research and Design, 187, 9-26.

[26] Kırbıyık, Ç., Pütün, A. E., & Pütün, E. (2017) Equilibrium, kinetic, and thermodynamic studies of the adsorption of Fe (III) metal ions and 2, 4-dichlorophenoxyacetic acid onto biomass-based activated carbon by ZnCl2 activation, Surfaces and Interfaces, 8, 182-192.

[27] Karagöz, S., Tay, T., Ucar, S., & Erdem, M. (2008) Activated carbons from waste biomass by sulfuric acid activation and their use on methylene blue adsorption, Bioresource technology, 99(14), 6214-6222.

[28] Rezazadeh, N., Danesh, S., & Eftekhari, M., (2023) Investigation the adsorption mechanism of a non-ionic surfactant on graphene oxide and its derivatives (kinetic, isotherm curves, thermodynamic, and effect of salts studies), Environmental Nanotechnology, Monitoring & Management, 20, 100819.

[29] Zhao, S., Zhan, Y., Wan, X., He, S., Yang, X., Hu, J., & Zhang, G., (2020) Selective and efficient adsorption of anionic dyes by core/shell magnetic MWCNTs nano-hybrid constructed through facial polydopamine tailored graft polymerization: Insight of adsorption mechanism, kinetic, isotherm and thermodynamic study, Journal of Molecular Liquids, 319, 114289.

[30] Ghasemi, N., Ghasemi, M., Moazeni, S., Ghasemi, P., Alharbi, N. S., Gupta, V. K., ... & Tkachev, A. G., (2018) Zn (II) removal by amino-functionalized magnetic nanoparticles: Kinetics, isotherm, and thermodynamic aspects of adsorption, Journal of industrial and engineering chemistry, 62, 302-310.

[31] Zhang, X., Yuan, N., Xu, S., Li, Y., & Wang, Q. (2022) Efficient adsorptive elimination of organic pollutants from aqueous solutions on ZIF-8/MWCNTs-COOH nanoadsorbents: Adsorption kinetics, isotherms, and thermodynamic study, Journal of Industrial and Engineering Chemistry, 111, 155-167.

[32] De Castro, M. L. F. A., Abad, M. L. B., Sumalinog, D. A. G., Abarca, R. R. M., Paoprasert, P., & de Luna, M. D. G., (2018) Adsorption of methylene blue dye and Cu (II) ions on EDTA-modified bentonite: isotherm, kinetic and thermodynamic studies, Sustainable Environment Research, 28(5), 197-205.

[33] Mbarki, F., Selmi, T., Kesraoui, A., & Seffen, M., (2022) Low-cost activated carbon preparation from Corn stigmata fibers chemically activated using H_3PO_4, $ZnCl_2$ and KOH: Study of methylene blue adsorption, stochastic isotherm and fractal kinetic, Industrial Crops and Products, 178, 114546.

[34] Mani, D., Elango, D., Priyadharsan, A., Al-Humaid, L. A., Al-Dahmash, N. D., Ragupathy, S., ... & Ahn, Y. H., (2023) Groundnut shell chemically treated with KOH to prepare inexpensive activated carbon: Methylene blue adsorption and equilibrium isotherm studies, Environmental Research, 231, 116026.

[35] Mandal, S., Calderon, J., Marpu, S. B., Omary, M. A., & Shi, S. Q., (2021) Mesoporous activated carbon as a green adsorbent for the removal of heavy metals and Congo red: Characterization, adsorption kinetics, and isotherm studies, Journal of Contaminant Hydrology, 243, 103869.

[36] Ahmad, M. A., Eusoff, M. A., Oladoye, P. O., Adegoke, K. A., & Bello, O. S., (2020) Statistical optimization of Remazol Brilliant Blue R dye adsorption onto activated carbon prepared from pomegranate fruit peel, Chemical Data Collections, 28, 100426.

[37] Rasli, N. I., Basri, H., & Harun, Z. (2020) Zinc oxide from aloe vera extract: two-level factorial screening of biosynthesis parameters, Heliyon, 6(1), e03156.

[38] Fanoro, O. T., Parani, S., Maluleke, R., Lebepe, T. C., Varghese, R. J., Mgedle, N., ... & Oluwafemi, O. S. (2021) Biosynthesis of smaller-sized platinum nanoparticles using the leaf extract of combretum erythrophyllum and its antibacterial activities, Antibiotics, 10(11), 1275.

[39] Md Salim, R., Asik, J., & Sarjadi, M. S. (2021) Chemical functional groups of extractives, cellulose and lignin extracted from native Leucaena leucocephala bark, Wood Science and Technology, 55, 295-313.

[40] Fernandes, J., Reboredo, F. H., Luis, I., Silva, M. M., Simões, M. M., Lidon, F. C., & Ramalho, J. C. (2022) Elemental Composition of Commercial Herbal Tea Plants and Respective Infusions, Plants, 11(11), 1412.

[41] Prajapati, C., Jolly, A., & Ravulapalli, S. (2020) Bio inspired synthesis of silver nanoparticles and its applications to spin–orbit interactions of light, Nano Express, 1(3), 030031.

[42] Faramitha, Y., Barori, F. R., Dimawarnita, F., Aqoma, H., Nugraha, A. F., & Ferdiansyah, A. (2023) Fabrication of glutathione-modified gold nanoparticles as 3-chloropropane-1, 2-diol sensor, Communications in Science and Technology, 8(1), 82-86.

[43] Goetze, J., & Weckhuysen, B. M. (2018) Spatiotemporal coke formation over zeolite ZSM-5 during the methanol-to-olefins process as studied with operando UV-vis spectroscopy: a comparison between H-ZSM-5 and Mg-ZSM-5, Catalysis Science & Technology, 8(6), 1632-1644.

[44] Santalucia, R., Vacca, T., Cesano, F., Martra, G., Pellegrino, F., & Scarano, D. (2020) Few-layered MoS_2 nanoparticles covering anatase TiO_2 nanosheets: Comparison between ex situ and in situ synthesis approaches, Applied Sciences, 11(1), 143.

[45] de Ménorval, L. C., Chaqroune, A., Coq, B., & Figueras, F. (1997) Characterization of mono-and bi-metallic platinum catalysts using CO FTIR spectroscopy Size effects and topological segregation, Journal of the Chemical Society, Faraday Transactions, 93(20), 3715-3720.

[46] Wu, W. C., Liao, L. F., Lien, C. F., & Lin, J. L. (2001) FTIR study of adsorption, thermal reactions and photochemistry of benzene on powdered TiO_2, Physical Chemistry Chemical Physics, 3(19), 4456-4461.

[47] Gaitán-Alvarez, J., Berrocal, A., Mantanis, G. I., Moya, R., & Araya, F. (2020) Acetylation of tropical hardwood species from forest plantations in Costa Rica: an FTIR spectroscopic analysis, Journal of Wood Science, 66(1), 49.

[48] Leksawasdi, N., Chaiyaso, T., Rachtanapun, P., Thanakkasaranee, S., Jantrawut, P., Ruksiriwanich, W., ... & Jantanasakulwong, K. (2021) Corn starch reactive blending with latex from natural rubber using Na^+ ions augmented carboxymethyl cellulose as a crosslinking agent, Scientific Reports, 11(1), 19250.

[49] Mutaillifu, P., Bobakulov, K., Abuduwaili, A., Huojiaaihemaiti, H., Nuerxiati, R., Aisa, H. A., & Yili, A. (2020) Structural characterization and antioxidant activities of a water soluble polysaccharide isolated from Glycyrrhiza glabra, International journal of biological macromolecules, 144, 751-759.

[50] Santiago Cintrón, M., & Hinchliffe, D. J. (2015) FT-IR examination of the development of secondary cell wall in cotton fibers, Fibers, 3(1), 30-40.

[51] Britto, A. S. F., Binoj, J. S., Mansingh, B. B., & Jass, P. N. (2023) Extensive characterization of novel cellulosic biofiber from leaf sheath of Licuala grandis for biocomposite applications, Biomass Conversion and Biorefinery, 1-10.

[52] Szmatoła, M., Chrobak, J., Grabowski, R., Iłowska, J., Woch, J., Szwach, I., ... & Grymel, M. (2018) Spectroscopic methods in the evaluation of modified vegetable base oils from Crambe abyssinica, Molecules, 23(12), 3243.

[53] Guzmán-Mendoza, J. J., Chávez-Flores, D., Montes-Fonseca, S. L., González-Horta, C., Orrantia-Borunda, E., & Sánchez-Ramírez, B. (2022) A Novel method for carbon nanotube functionalization using immobilized candida antarctica lipase, Nanomaterials, 12(9), 1465.

[54] Geminiani, L., Campione, F. P., Corti, C., Luraschi, M., Motella, S., Recchia, S., & Rampazzi, L. (2022) Differentiating between Natural and Modified Cellulosic Fibres Using ATR-FTIR Spectroscopy, Heritage, 5(4), 4114-4139.

[55] Lu, Y., Liu, L., Shen, D., Yang, C., & Zhang, L. (2004) Infrared study on in situ polymerization of zinc dimethacrylate in poly (α-octylene-co-ethylene) elastomer, Polymer international, 53(6), 802-808.

[56] Singh, O., Khanam, Z., Misra, N., & Srivastava, M. K. (2011) Chamomile (Matricaria chamomilla L.): an overview, Pharmacognosy reviews, 5(9), 82.

[57] Liu, Q., Ye, M., Yu, G., & Han, A. (2023) Synthesis of octavinyl polyhedral oligomeric silsesquioxane (ovi-POSS) based organic/inorganic hybrid resin microspheres for rapid and efficient oils absorption, Journal of Applied Polymer Science, 140(6), e53429.

[58] Mohtashami, S., Asasian Kolur, N., Kaghazchi, T., Asadi-Kesheh, R., & Soleimani, M. (2018) Optimization of sugarcane bagasse activation to achieve adsorbent with high affinity towards phenol, Turkish Journal of Chemistry, 42(6), 1720-1735.

[59] Kang, E. J., Baek, Y. M., Hahm, E., Lee, S. H., Pham, X. H., Noh, M. S., ... & Jun, B. H. (2019) Functionalized β-cyclodextrin immobilized on Ag-embedded silica nanoparticles as a drug carrier, International Journal of Molecular Sciences, 20(2), 315.

[60] Puziy, A. M., Poddubnaya, O. I., Sobiesiak, M., & Gawdzik, B. (2017) Assessment of the structural evolution of polyimide-derived carbons obtained by phosphoric acid activation using Fourier transform infrared and Raman spectroscopy, Adsorption Science & Technology, 35(5-6), 403-412.

[61] Li, Y., Zhang, X., Yang, R., Li, G., & Hu, C. (2015) The role of H_3PO_4 in the preparation of activated carbon from NaOH-treated rice husk residue, RSC advances, 5(41), 32626-32636.

[62] Sajjadi, B., Chen, W. Y., Mattern, D. L., Hammer, N., & Dorris, A. (2020) Low-temperature acoustic-based activation of biochar for enhanced removal of heavy metals, Journal of Water Process Engineering, 34, 101166.

[63] Harja, M., Buema, G., Lupu, N., Chiriac, H., Herea, D. D., & Ciobanu, G., (2020) Fly ash coated with magnetic materials: Improved adsorbent for Cu (II) removal from wastewater, Materials, 14(1), 63.

[64] Ewis, D., Mahmud, N., Benamor, A., Ba-Abbad, M. M., Nasser, M., & El-Naas, M., (2022) Enhanced Removal of Diesel Oil Using New Magnetic Bentonite-Based Adsorbents Combined with Different Carbon Sources, Water, Air, & Soil Pollution, 233(6), 195.

[65] Jawad, A. H., Saber, S. E. M., Abdulhameed, A. S., Farhan, A. M., ALOthman, Z. A., & Wilson, L. D., (2023) Characterization and applicability of the natural Iraqi bentonite clay for toxic cationic dye removal: Adsorption kinetic and isotherm study, Journal of King Saud University-Science, 35(4), 102630.

[66] Atif, M., Haider, H. Z., Bongiovanni, R., Fayyaz, M., Razzaq, T., & Gul, S., (2022) Physisorption and chemisorption trends in surface modification of carbon black, Surfaces and Interfaces, 102080.

[67] Debnath, S., & Das, R., (2023) Strong adsorption of CV dye by Ni ferrite nanoparticles for waste water purification: Fits well the pseudo second order kinetic and Freundlich isotherm model, Ceramics International, 49(10), 16199-16215.

[68] Khamwichit, A., Dechapanya, W., & Dechapanya, W., (2022) Adsorption kinetics and isotherms of binary metal ion aqueous solution using untreated venus shell, Heliyon, 8(6), e09610.

[69] Akdemir, M., Isik, B., Cakar, F., & Cankurtaran, O., (2022) Comparison of the adsorption efficiency of cationic (Crystal Violet) and anionic (Congo Red) dyes on Valeriana officinalis roots: Isotherms, kinetics, thermodynamic studies, and error functions, Materials Chemistry and Physics, 291, 126763.

[70] Nasiri, A., Rajabi, S., Amiri, A., Fattahizade, M., Hasani, O., Lalehzari, A., & Hashemi, M., (2022) Adsorption of tetracycline using $CuCoFe_2O_4$@ Chitosan as a new and green magnetic nanohybrid adsorbent from aqueous solutions: Isotherm, kinetic and thermodynamic study, Arabian Journal of Chemistry, 15(8), 104014.

[71] Farooq, S., Al Maani, A. H., Naureen, Z., Hussain, J., Siddiqa, A., & Al Harrasi, A., (2022) Synthesis and characterization of copper oxide-loaded activated carbon nanocomposite: Adsorption of methylene blue, kinetic, isotherm, and thermodynamic study, Journal of Water Process Engineering, 47, 102692.

[72] Kumbhar, P., Narale, D., Bhosale, R., Jambhale, C., Kim, J. H., & Kolekar, S., (2022) Synthesis of tea waste/Fe_3O_4 magnetic composite (TWMC) for efficient adsorption of crystal violet dye: Isotherm, kinetic and thermodynamic studies, Journal of Environmental Chemical Engineering, 10(3), 107893.

[73] Bassam, R., El Alouani, M., Maissara, J., Jarmouni, N., Belhabra, M., Chbihi, M. E. M., & Belaaouad, S., (2022) Investigation of competitive adsorption and desorption of heavy metals from aqueous solution using raw rock: Characterization kinetic, isotherm, and thermodynamic, Materials Today: Proceedings, 52, 158-165.

[74] Sadeghi, M., Moradian, M., Tayebi, H. A., & Mirabi, A., (2023) Removal of Penicillin G from aqueous medium by PPI@ SBA-15/ZIF-8 super adsorbent: Adsorption isotherm, thermodynamic, and kinetic studies, Chemosphere, 311, 136887.

[75] Song, X., Ma, X., & Zeng, Y., (2017) Adsorption equilibrium and thermodynamics of CO_2 and CH_4 on carbon molecular sieves, Applied Surface Science, 396, 870-878.

[76] Ghosh, K., Bar, N., Biswas, A. B., & Das, S. K. (2021) Elimination of crystal violet from synthetic medium by adsorption using unmodified and acid-modified eucalyptus leaves with MPR and GA application, Sustainable Chemistry and Pharmacy, 19, 100370.

[77] Ali, N. S., Jabbar, N. M., Alardhi, S. M., Majdi, H. S., & Albayati, T. M. (2022) Adsorption of methyl violet dye onto a prepared bio-adsorbent from date seeds: Isotherm, kinetics, and thermodynamic studies, Heliyon, 8(8), e10276.

[78] Oloo, C. M., Onyari, J. M., Wanyonyi, W. C., Wabomba, J. N., & Muinde, V. M. (2020) Adsorptive removal of hazardous crystal violet dye form aqueous solution using Rhizophora mucronata stem-barks: Equilibrium and kinetics studies, Environmental Chemistry and Ecotoxicology, 2, 64-72.

[79] Dabagh, A., Bagui, A., Abali, M. H., Aziam, R., Chiban, M., Sinan, F., & Zerbet, M. (2021) Adsorption of Crystal Violet from aqueous solution onto eco-friendly native Carpobrotus edulis plant, Materials Today: Proceedings, 37, 3980-3986.

[80] Senthilkumaar, S., Kalaamani, P., & Subburaam, C. V. (2006) Liquid phase adsorption of crystal violet onto activated carbons derived from male flowers of coconut tree, Journal of hazardous materials, 136(3), 800-808.

[81] Ji, Q., & Li, H. (2021) High surface area activated carbon derived from chitin for efficient adsorption of Crystal Violet, Diamond and Related Materials, 118, 108516.

[82] Rani, S., & Chaudhary, S. (2022) Adsorption of methylene blue and crystal violet dye from waste water using Citrus limetta peel as an adsorbent, Materials Today: Proceedings, 60, 336-344.

[83] Yusuff, A. S., Ajayi, O. A., & Popoola, L. T. (2021) Application of Taguchi design approach to parametric optimization of adsorption of crystal violet dye by activated carbon from poultry litter, Scientific African, 13, e00850.

[84] Kamath, A. A., Nayak, N. G., & Sagar, R. (2021) Coconut flower sheath derived activated charcoal as efficient and cost effective adsorbent for crystal violet dye removal, Inorganic Chemistry Communications, 134, 109077.